Global Journal of Engineering and Technology Advances

eISSN: 2582-5003

Cross Ref DOI: 10.30574/gjeta

Journal homepage: https://gjeta.com/

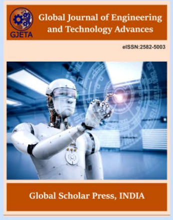

(RESEARCH ARTICLE)

Check for updates

Development of an IoT-Enabled Electronic Hospital Bed with Integrated Patient Monitoring for Resource-Constrained Settings

Abdullateef Ogundipe [1, 2, *], Abdul Rasak Zubair [1], Oluwamuyiwa Emmanuel Obakin [1], Emmanuel Adeyemi Adebisi [3], James Udoh Imoh [1], Abubakr Olaniyi Zubair [4], Victor Oluwatimilehin Omotoso [1], Ifeanyi Theodore Anigbogu [1] and Allison Lekwa Onyeije [1]

[1] *Department of Electrical and Electronic Engineering, University of Ibadan, Ibadan, Nigeria;*

[2] *Department of Automatic Control., LAMIH, Université Polytechnique Hauts-de-France, Valenciennes, France.*

[3] *Department of Electrical and Electronics Engineering, University of Ilorin, Ilorin, Nigeria.*

[4] *Department of Electrical and Electronics Engineering, Olabisi Onabanjo University, Ago-Iwoye, Nigeria.*

Global Journal of Engineering and Technology Advances, 2026, 27(03), 159-170

Publication history: Received on 07 May 2026; revised on 14 June 2026; accepted on 17 June 2026

Article DOI: https://doi.org/10.30574/gjeta.2026.27.3.0158

Abstract

Hospital beds are central to modern clinical care, yet sub-Saharan healthcare systems still rely largely on manually operated frames that lack automated positioning, integrated patient monitoring, and resilience to unstable power supply. This paper presents the design and implementation of an Internet-of-Things (IoT)-enabled electronic hospital bed engineered for the operational realities of Nigerian healthcare facilities. The system integrates a custom mild-steel articulated frame, two 12 V linear actuators, an ESP32-WROOM-32 microcontroller, a suite of environmental / biomedical sensors for heart rate, SpO_2, body temperature, room temperature and room humidity, an ESP32-CAM module for visual telepresence, and a hybrid mains-and-battery power architecture with a 12 V 80 Ah lead-acid backup. In addition to bedside control, a custom web dashboard provides remote bidirectional control and real-time visualization of patient vitals on computer systems or smart phones. Experimental evaluation revealed a vertical lift velocity of 6.35 mm/s, finite-element predicted factor of safety of 1.37 against a 1,737 N service load, command-to-action latency of 180ms, emergency-stop response below 50ms, sensor accuracy within manufacturer specifications, power-conversion efficiency of 86.27 %, and a battery autonomy exceeding 32 hours under typical intermittent clinical use. The prospect of clinically relevant electromechanical and IoT functionality using locally sourced materials and components for patient care in resource-constrained settings has been demonstrated.

Keywords: Hospital bed; Internet of Things (IoT); Patient care; Vital signs monitoring; Electronics; Resource-constrained settings

1. Introduction

The hospital bed is one of the most fundamental units of clinical infrastructure, it supports patient rest, therapy delivery, monitoring, and post-operative recovery [1]. It is typically occupied by patients for the entirety of their hospitalization. Over the last century, hospital beds have evolved from rudimentary wooden frames to iron-framed manual cranks, then to motorized electric beds, and most recently to smart beds that combine motorized positioning with embedded sensing, networked communication, and decision-support intelligence [2]. This evolution reflects a broader shift in clinical practice from reactive bedside care to continuous, data-driven patient management. Despite these advances, the global distribution of bed technology remains highly uneven. The World Health Organization reports that hospital bed densities in sub-Saharan Africa are typically less than half of the global average, and the Nigerian system in particular operates at approximately 0.9 beds per 1,000 population against a global average of about 2.3 beds per 1,000 [3]. The

* Corresponding author: A. Ogundipe

shortage is compounded by the predominance of manual beds that lack height adjustment, trendelenburg, reverse-trendelenburg articulation, and any form of integrated monitoring. The resulting limitations, inadequate adjustability, absent vital-sign tracking, slow emergency repositioning, caregiver musculoskeletal strain, and sensitivity to unreliable mains electricity, contribute to delayed interventions and avoidable adverse events in resource-constrained wards [4].

Modern smart hospital beds incorporate multiple sensing modalities to enable continuous, non-invasive patient monitoring without imposing additional bedside equipment [2]. Pressure-sensor arrays embedded in the mattress monitor body-pressure distribution and provide alerts for repositioning, reducing the incidence of pressure ulcers in immobilized patients [5]. Fibre Bragg Grating (FBG) optical sensors, embedded in the mattress core, transduce micro-vibrations from heart and respiration into wavelength shifts and provide ballistocardiograph monitoring without skin-contact electrodes [6]. Bed-exit detection, implemented through load cells or capacitive proximity sensing, alerts nursing staff when high-fall-risk patients attempt to leave the bed unassisted [7]. Integrated vital-sign monitors, typically photoplethysmography (PPG) sensors for heart rate and SpO_2, digital thermometers for body temperature, and ambient sensors for ward conditions replace the discrete monitors traditionally wheeled to the bedside [5]. Internet of Things (IoT) connectivity binds these sensors into a coherent data-acquisition platform; sensor outputs are streamed to local edge computers, cloud servers, or hospital information system. They support real-time dashboards, longitudinal trend analysis, and machine-learning-based decision making [8]. The combination of mechanical automation and continuous sensing redefines the hospital bed as an active node in the patient-care workflow, rather than a passive piece of furniture [9,10].

The Nigerian biomedical-engineering landscape, traced back to the 1970s, has historically been constrained by an emphasis on equipment importation and servicing rather than indigenous design and manufacture. The medical instruments designed for temperate environments often fail prematurely in tropical African hospitals [11]. The consequences of equipment breakdown, untreated patients, wrong diagnosis, and overloaded repair shops, compound the underlying shortage of devices [11]. Locally developed biomedical instruments interfaced with web-based telediagnosis platforms can extend specialist expertise beyond particular health care centers [12, 13].

The operational reality of large Nigerian referral centers reinforces these arguments. University College Hospital (UCH), Ibadan, the country's premier teaching hospital can only boast of 1,445 bed spaces which are not adequate for the patient population [14]. Studies of resource utilization in southeastern Nigerian teaching hospitals have similarly shown chronic over-utilization of bed capacity with simultaneous shortfalls in supporting equipment [4]. The COVID-19 pandemic accelerated awareness of this inadequacy, especially for vulnerable populations, and underscored the importance of locally adapted, contact-minimizing medical devices [15, 16]. Any electronic bed that is to be useful in such an environment must therefore be inexpensive, locally maintainable, energy-efficient, and resilient to extended grid outages. Studies on Nigerian populations have further highlighted that hospital beds imported from temperate manufacturers are often dimensionally inappropriate for local patients, leading to ergonomic mismatch for both patients and caregivers [17, 18]. Local development of hospital beds and biomedical devices in general remain an active area of research to bridge the gap between demand and supply of these devices. The development of an IoT-enabled electronic hospital bed is presented.

2. Design and methodology

2.1. System Architecture Overview

The smart electronic hospital bed comprises of subsystems: a mechanical frame and electromechanical actuation unit, an embedded control and biomedical-sensing unit, a hybrid power-management unit, and an IoT communication layer with a web-based user interface. These subsystems are coordinated by a single ESP32-WROOM-32 microcontroller acting as the central controller. The ESP32 receives commands from physical pushbuttons or from the web dashboard, drives two linear actuators through dedicated driver circuits, continuously samples the biomedical and environmental sensors, and streams the resulting data, together with a JPEG video feed from a separate ESP32-CAM module, to caregivers. The complete information flow and inter-subsystem relationships are illustrated in Figure 1.

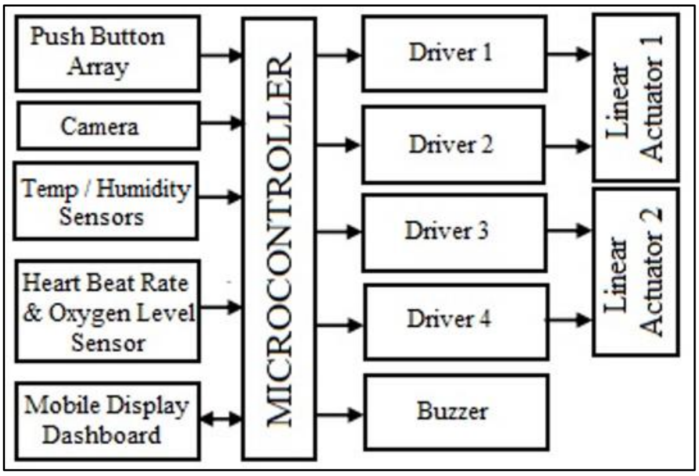

Figure 1 System architecture diagram of the project

2.2. Mechanical Frame

The mechanical frame is the structural foundation of the bed and must support both the patient and all electromechanical components while permitting the articulation required for clinical positioning. The frame was modelled in AutoCAD 2023 and fabricated from mild-steel box sections (25 mm × 25 mm × 2 mm for the main frame and 20 mm × 20 mm × 1.5 mm for cross-supports). Overall dimensions of 1,400 mm × 700 mm with a height-adjustment range of 450–750 mm was chosen on the basis of Nigerian pediatric anthropometric data [9], [10]. The isometric view, the side view, and the front view are in Figure 2 (a), (c), and (g) respectively. Figure 2 (c) and (e) show the side view with horizontal normal positioning; Figure 2(e) is the minimum level. Figure 2 (d) and (f) show the side view with trendelenburg positioning and reverse-trendelenburg positioning respectively. The trendelenburg positioning is also known as back-tilt (BTILT) while the reverse-trendelenburg positioning is also known as forward-tilt (FTILT).

The frame incorporates two articulation zones that together provide four degrees of freedom. Vertical height adjustment along the Y-axis is achieved by two synchronized 12 V DC linear actuators mounted at the head and foot ends; coordinated firmware control of these actuators maintains level elevation across a 300 mm range. Trendelenburg and reverse-trendelenburg positioning is realized by the two actuators being operated in reverse directions beneath the frame.

The structural reliability under realistic loading was verified by the frame being analyzed using SolidWorks Simulation. A combined service load of 1,737 N, derived from a 100 kg patient and the 18 kg frame, multiplied by a 1.5 dynamic factor to model transient effects during repositioning was applied to the mattress platform. The simulation predicted a maximum von Mises stress of 182 MPa in critical support members, well below the 250 MPa yield strength of the mild steel and giving a factor of safety (FoS), as defined by (1), of 1.37, where σ_Y = 250 MPa is the yield strength of the mild steel and σ_{max} = 182 MPa is the maximum predicted von Mises stress. The maximum vertical deflection was 6.8 mm, within accepted serviceability limits for medical beds. To complement this structural margin, the hardware integrates internal limit switches in every actuator to prevent over-extension, ball-joint mounting brackets to accommodate angular changes without binding, and gusset-plate reinforcements at high-stress welded joints to redistribute load.

$$FoS = \frac{\sigma_Y}{\sigma_{max}} = \frac{250\ MPa}{182\ MPa} \approx 1.37 \qquad (1)$$

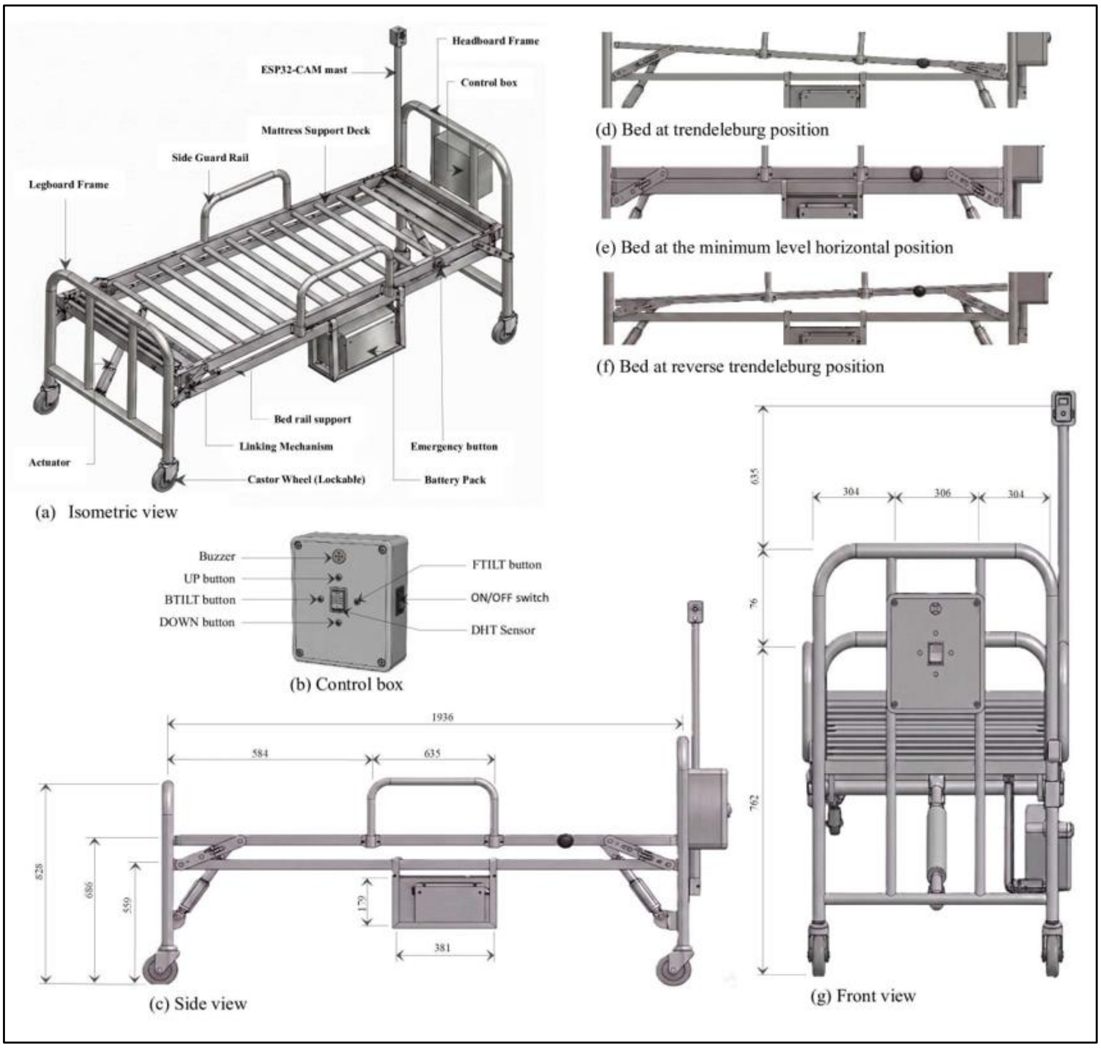

Figure 2 Several views of the Mechanical Frame Design

2.3. Electronic Subsystem

The electronic subsystem implements all real-time control, sensing, and communication functions of the bed. It is built around an ESP32-WROOM-32 microcontroller, with peripheral driver, sensor, telepresence, and user-interface modules connected to dedicated GPIO pins as shown in Figure 3.

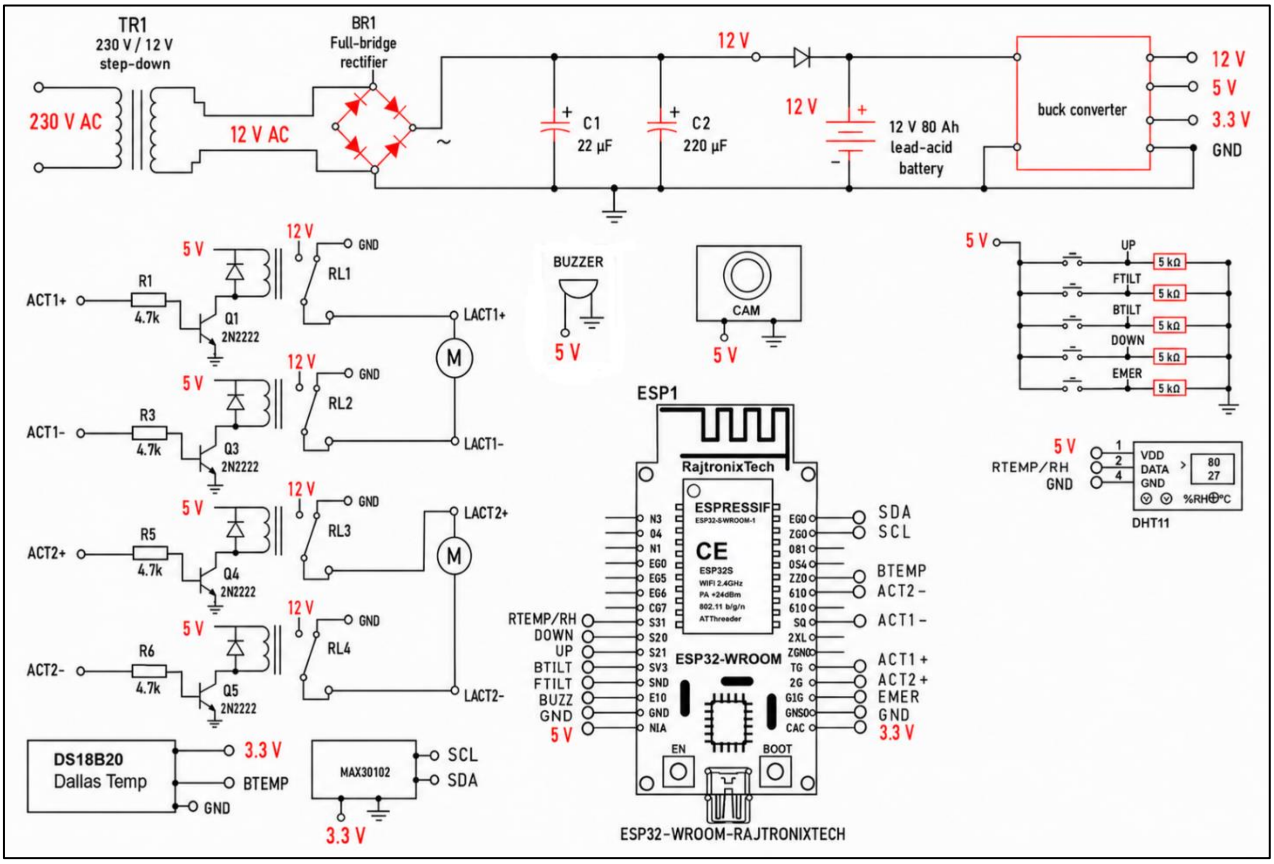

Figure 3 Complete circuit schematic of the electronic subsystem

2.3.1. Microcontroller and Actuator Drive Circuits

The ESP32-WROOM-32 was selected over alternatives such as the ATmega2560-based Arduino Mega for three principal reasons, its dual-core Xtensa LX6 architecture permits true concurrent execution of safety-critical and non-critical tasks; its integrated Wi-Fi (802.11 b/g/n) and Bluetooth (v4.2 BR/EDR and BLE) eliminate the cost and bulk of external communication shields and its 240 MHz clock provides an order-of-magnitude headroom over Arduino-class controllers for concurrent sensor sampling and HTTP server duties.

In the firmware partitioning adopted here, Core 0 handles safety-critical activities, emergency-stop monitoring with a sub-50 ms response budget and actuator-state sequencing, while Core 1 handles sensor acquisition, web-server requests, and Wi-Fi housekeeping. Each linear actuator is driven through an H-bridge-equivalent driver circuit comprising two 2N2222 NPN bipolar junction transistors (BJTs), two 12 V SPDT 10 A relays, 1N4007 flyback diodes for inductive-spike suppression, and 4.7 kΩ base resistors.

The BJTs translate the 3.3 V GPIO logic level to the relay-coil drive level, while the relays in turn switch the 12 V / up to 4.5 A actuator current and reverse polarity to enable bidirectional travel. Four such driver circuits are wired in two complementary pairs (one pair per actuator) so that the microcontroller can extend or retract each actuator without contention. Software interlocks in the firmware prevent simultaneous activation of conflicting directions, protecting both the relays and the mechanical frame. The driver topology for the two actuators is shown in Figure 3.

2.3.2. Biomedical and Environmental Sensors

Three sensors form the bed's integrated monitoring suite. The MAX30102 is a high-sensitivity, integrated pulse-oximetry and heart-rate (HR) module that uses photoplethysmography (PPG); two LEDs at 660 nm (red) and 880 nm (infrared) illuminate the skin while a low-noise photodetector measures reflected light. Heart rate is derived from the rhythmic light-absorption changes induced by arterial pulsation, and SpO_2 is computed from the ratio of red to infrared absorption, exploiting the differing optical properties of oxygenated and deoxygenated haemoglobin. The module communicates with the ESP32 over an I^2C bus at 400 kHz, samples PPG at 100 Hz, and provides factory-calibrated heart-rate (HR) accuracy of ±3 bpm and SpO_2 accuracy of ±2 %. A 32-sample on-chip FIFO buffer allows the microcontroller to process data in batches, conserving processor cycles.

The DS18B20 (Dallas) is a 1-Wire digital thermometer used for body-temperature (BTEMP) measurement. It provides ±0.5 °C accuracy across the clinically relevant range (35–42 °C), 12-bit resolution (0.0625 °C), and a conversion time below 750 ms. The waterproof stainless-steel probe variant is well suited to medical contact, and the 1-Wire interface allows the cable to extend from the bed control box to the patient without signal-integrity loss. Compared with analogue sensors such as the LM35, the DS18B20's digital output is immune to motor-induced noise on the bed wiring.

The DHT11 ambient sensor monitors ward conditions, providing temperature (0–50 °C, ±2 °C) and relative humidity (20–90 %, ±5 %) over a single-wire digital interface at 1 Hz. Although less precise than the DS18B20, it is inexpensive, requires only one digital pin, and is sufficient for contextual interpretation of the patient's vitals (for example, distinguishing fever from environmental heat stress). The arrangement of the three sensors and their isolation from the high-power actuator wiring is also shown in Figure 3.

2.3.3. Visual Telepresence Module

Visual telepresence is provided by an ESP32-CAM module fitted with an OV2640 2-megapixel CMOS image sensor (1600 × 1200 maximum, 25 fps at VGA). The module is mounted on the mechanical frame as illustrated in Figure 2 and operates as an independent Wi-Fi node that streams JPEG-compressed frames over HTTP. The web dashboard embeds the stream in an iframe so that clinicians can visually inspect the patient remotely, for example to assess level of consciousness, breathing pattern, or evidence of distress, thus providing the qualitative dimension of telediagnosis that complements the quantitative sensor data, as proposed in [6].

2.3.4. User Interface and Pushbutton Array

A tactile pushbutton array provides the primary local user interface for caregivers and patients. It comprises five momentary buttons, UP, DOWN, FORWARD-TILT (FTILT), BACK-TILT (BTILT), and EMERGENCY (EMER), connected to GPIO pins on the ESP32-WROOM. These pins are explicitly chosen to be input-only on the ESP32, eliminating the risk of accidental output configuration during firmware development. External 10 kΩ pull-up resistors are added to provide noise immunity against electromagnetic interference from the actuator motor brushes. The EMER button is wired to a hardware interrupt that overrides software state, immediately halting all relay activity and sounding a buzzer. Figure 2(b) shows the UP, DOWN, FTILT, and BTILT push buttons, the ON/OFF switch, the Buzzer, and the DHT11 sensor. The EMER push button is shown in Figure 2(a).

2.4. Power Management Subsystem

The power-management subsystem is engineered specifically for the unstable mains environment characteristic of Nigerian healthcare facilities. It implements a two-source hybrid architecture: a primary path drawing from the 220 V AC mains and a secondary path drawing from a 12 V 80 Ah lead-acid deep-cycle battery. On the primary path, a 220 V/12 V step-down transformer feeds a full-bridge rectifier and a smoothing capacitor to produce a regulated 12 V DC bus that simultaneously charges the battery and powers the actuator drivers. A buck-converter stage steps the 12 V bus down to the 5 V and 3.3 V rails required by the ESP32, sensors, and camera.

Battery charging is performed at approximately 4.5 A, well within the recommended 0.1 C rate (8 A) for an 80 Ah lead-acid cell, so as to preserve battery life under the high-cycle conditions expected in a ward. The total battery energy is given by (2); $V_{\beta att}$ is the nominal battery voltage and $C_{\beta att}$ is the rated amp-hour capacity. Under worst-case simultaneous operation of two actuators and the continuous electronics load, the maximum instantaneous load is obtained from (3); P_{act} = 54 W is the rated mechanical power of one linear actuator and P_{elec} ≈ 6 W is the continuous electronics load. The corresponding theoretical battery autonomy is given by (4). Under typical clinical use, however, actuators operate only for short bursts (≈ 20–30 s) when patients are repositioned; the time-averaged load drops to roughly 12 W, extending the practical autonomy to over 32 hours, as confirmed by the experimental results in section 3.4.

$$E_{\beta att} = V_{\beta att} \times C_{\beta att} = 12\,V \times 80\,Ah = 960\,Wh \quad (2)$$

$$P_{loadmax} = 2P_{act} \times P_{elec} = 2 \times 54\,W + 6\,W = 114\,W \quad (3)$$

$$t_{autonomy} = \frac{E_{\beta att}}{P_{loadmax}} = \frac{960\,Wh}{114\,W} \approx 8.4\,h \quad (4)$$

2.5. Embedded Firmware and Algorithm Design

The embedded firmware was developed in C/C++ within the Arduino IDE with the ESP32 board-support package. It is organized as a finite-state machine in which the system traverses well-defined states, IDLE, TILT_UP, TILT_DOWN, ALL_UP, ALL_DOWN, and EMERGENCY_STOP, under the joint control of the push button inputs and the web dashboard. A hardware watchdog timer guards against firmware hangs, while the dual-core partitioning keeps actuator and emergency-stop logic isolated from the latency-variable Wi-Fi stack.

Three core algorithms govern run-time behavior. The sensor-monitoring algorithm continuously reads the MAX30102, DS18B20, and DHT11, compares each value against preset clinical ranges, and triggers a buzzer alert and dashboard warning if a reading falls outside the safe band, as illustrated in Figure 4. The telepresence algorithm captures camera frames at the ESP32-CAM, streams them over HTTP to the dashboard, and similarly raises an alert if connectivity is lost as shown in Figure 5. The emergency-button algorithm is implemented as an interrupt service routine; pressing the EMER button immediately halts every relay, sounds the buzzer, and pushes a warning notification to the dashboard until a caregiver issues a manual reset as shown in Figure 6.

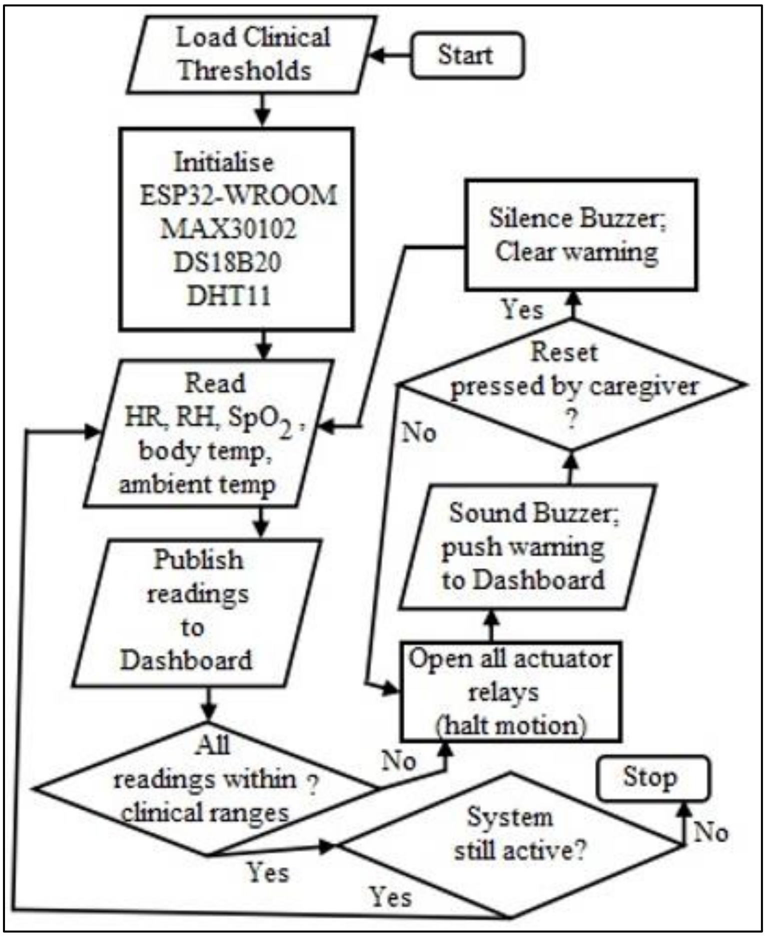

Figure 4 Sensor-monitoring algorithm flowchart

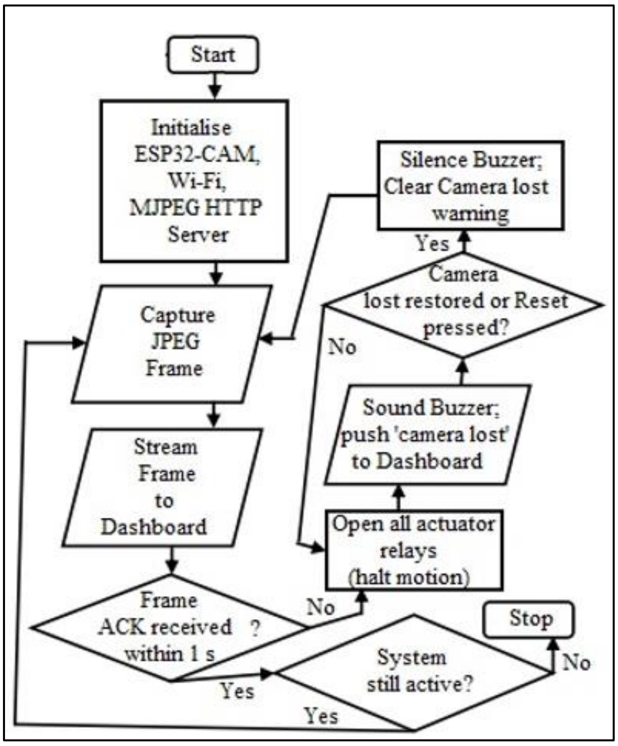

Figure 5 Camera-streaming algorithm flowchart

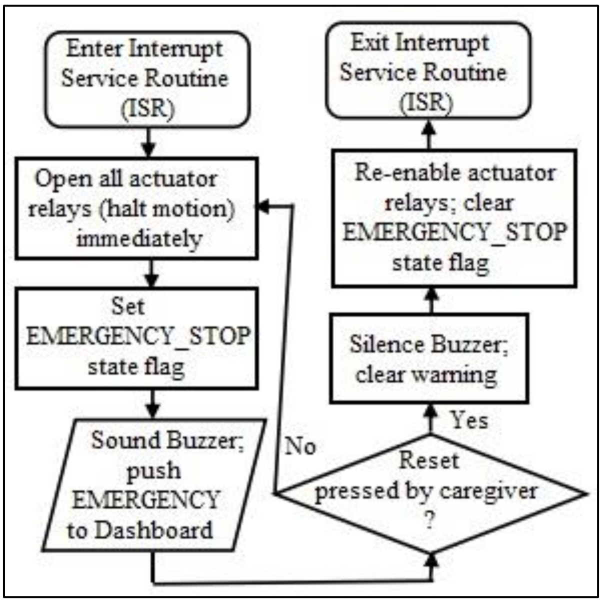

Figure 6 Emergency-button interrupt-handler flowchart

2.6. IoT Communication and Web Dashboard

The IoT subsystem turns the bed into a self-contained, locally networked telediagnosis station. The ESP32 hosts an asynchronous HTTP server that exposes two classes of endpoints: GET endpoints that return the most recent sensor readings as JSON, and POST endpoints that accept bed-positioning commands. A custom web dashboard polls these endpoints at 1 Hz, plots vital-sign trends, and provides large, color-coded buttons for caregivers to drive the bed. The dashboard layout, with status cards for body temperature (BTEMP), heart rate, blood oxygen (SpO_2), and environmental conditions [room temperature (RTEMP) and room humidity (RH)], is shown in Figure 7(a) and (b) for the Web Dashboard on a computer system and a smart phone respectively. Figure 8 show some views of the constructed hospital bed.

The end-to-end command pathway proceeds in four phases. In the command phase, the caregiver presses a button on the dashboard. In the transmission phase, JavaScript sends an HTTP GET/POST request over local Wi-Fi to the ESP32. In the execution phase, the ESP32 validates the request against safety limits (such as maximum lift travel and lockout of conflicting directions) and triggers the appropriate driver circuits. Finally, in the feedback phase, the ESP32 returns a success or error response, and the dashboard updates its status indicators. The embedded ESP32-CAM stream is rendered through an iframe element on the dashboard, providing the live visual feed without additional client-side software.

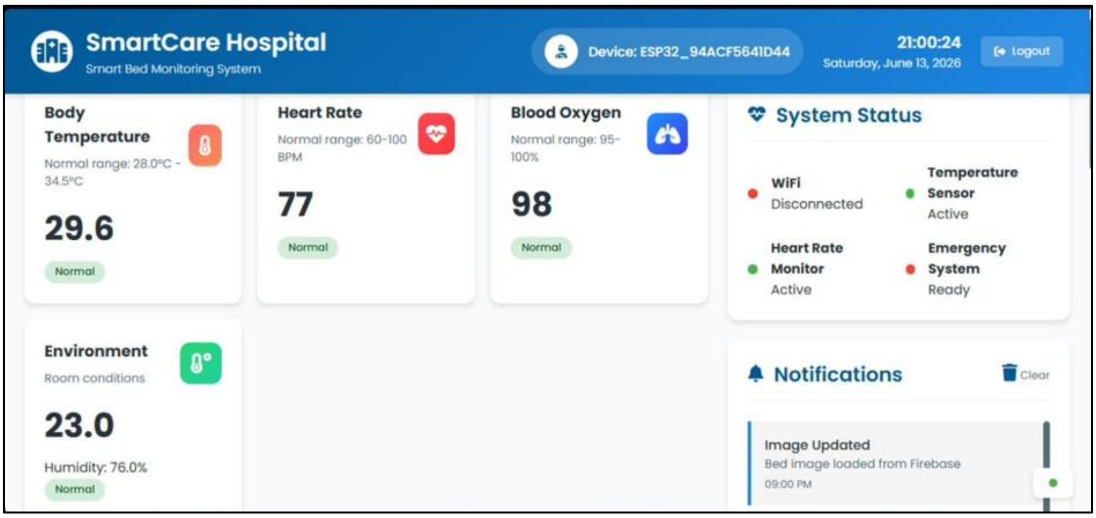

Web Dashboard on a Computer System

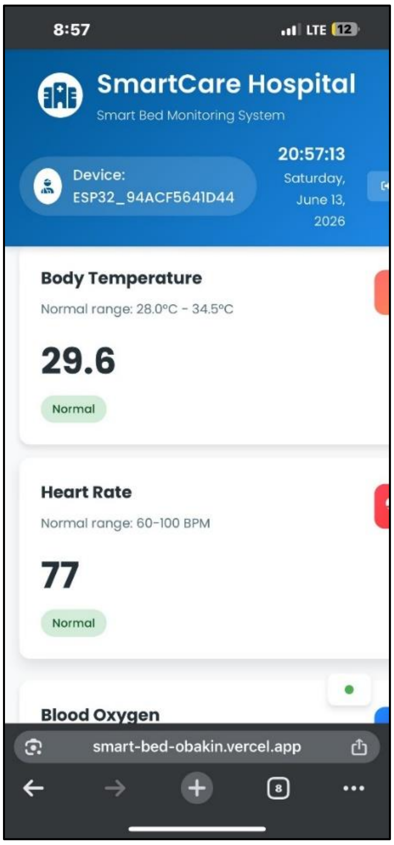

(b) Web Dashboard on a Smart phone

Figure 7 Dashboard showing real-time vitals, environmental data, and control panel


(a) Contro box (front view) (b) Side view (horizontal positioning)


(c) Reverse-trendelenburg positioning (forward-tilt) (d) Trendelenburg positioning (back-tilt)


(e) Actuator 1 (attached to the Headboard Frame) (e) Actuator 2 (attached to the Legboard Frame)

Figure 8 Some views of the constructed hospital bed

3. Results and discussion

The fully assembled prototype was evaluated through a structured testing regime covering mechanical performance, electronic and sensor accuracy, communication behaviour, power-system robustness, and integrated system usability. Each subsection below reports the observed quantitative metrics and compares them with the corresponding design targets.

3.1. Mechanical Performance

The vertical lift velocity was measured by timing the actuator stroke over its full 4.5-inch (114.3 mm) travel: 18 s of continuous operation yielded a velocity of 114.3 / 18 ≈ 6.35 mm/s. The two synchronized lift actuators maintained a level mattress platform with less than 2° deviation, as verified using a digital inclinometer. Trendelenburg and reverse-trendelenburg configurations were stable at ±15° of tilt, and the head and leg sections were independently elevated to their full 30° design targets. Static load testing with a 100 kg dummy patient produced a measured frame deflection of 3.1 mm, in close agreement with the Finite Element Analysis (FEA) prediction of 3.2 mm. After 100 complete movement cycles spanning all four degrees of freedom, no weld cracks, deformation, or actuator failures were observed.

3.2. Sensors' Accuracy

Sensor accuracy was validated against clinical reference instruments. Heart-rate measurements from the MAX30102 were compared with a calibrated finger pulse oximeter on five subjects across 50 readings, yielding a mean absolute error of 2.1 bpm against the manufacturer's ±3 bpm specification. SpO_2 readings showed a mean absolute error of 1.4 % against the ±2 % specification. Body-temperature measurements from the DS18B20, validated against a clinical mercury thermometer, showed a mean absolute error of 0.3 °C across the clinical range. The DHT11 remained within its quoted ±2 °C / ±5 % envelope across the test ward conditions.

3.2.1. Communication and Telediagnosis Performance

During a continuous 7-day operational test on a local Wi-Fi network, the bed maintained 99.2 % connection uptime. Command-to-action latency, timed from a dashboard button press to the start of actuator motion, averaged 180 ms over 100 trials with a range of 145–220 ms. The 1 Hz sensor-data polling exhibited less than 5 % packet loss. The ESP32-CAM streamed JPEG frames at approximately 20 fps at 640 × 480 resolution, with end-to-end latency below 500 ms adequate for remote clinical observation but not for fine-grained motion analysis. The web dashboard rendered correctly on Android smartphones, Windows laptops, and a tablet, confirming the cross-platform suitability of the responsive HTML/CSS design.

3.3. Power System Performance

The buck-converter stage was characterized at the steady-state electronics load. With an input of 12.6 V at 0.23 A (P_{in} = 2.898 W) and an output of 5.0 V at 0.50 A (P_{out} = 2.500 W), the conversion efficiency, defined by (5), was 86.27 %. The thermal rise of the regulator stabilized at 38 °C above ambient under continuous operation with passive heat-sink cooling. Battery autonomy testing confirmed 8.4 hours of continuous operation under the 30 W average load corresponding to a 50 % actuator duty cycle, in agreement with the theoretical estimate of Section 2.4. Under the more realistic intermittent-use profile (5 minutes of actuator activity per hour), autonomy exceeded 32 hours before the test was terminated, ample margin against the kind of multi-day grid outage observed at UCH Ibadan in late 2024. The automatic transfer switch from mains to battery operated reliably below 50 ms across all simulated mains failures, with no observable interruption of microcontroller or actuator activity.

$$\eta = \frac{P_{out}}{P_{in}} \times 100\,\% = \frac{2.500\,W}{2.898\,W} \times 100\,\% = 86.27\,\% \qquad (5)$$

3.4. Integrated System Validation

End-to-end tests confirmed seamless coordination across the mechanical, electronic, and software subsystems. Caregivers could intuitively manipulate the bed through the dashboard while observing live vital signs and the camera feed; positional commands were honored at the expected latency, and out-of-range physiological readings reliably triggered the buzzer and a corresponding warning card on the dashboard. The prototype was demonstrated successfully with a 25 kg pediatric mannequin, satisfying the project scope.

4. Conclusion

The prospect of local design and construction of smart hospital bed using locally available materials and components has been demonstrated. Performance that is clinically acceptable for resource-constrained wards have been achieved. These results demonstrate that clinically meaningful smart-bed functionality, automated multi-position adjustment, continuous monitoring, telepresence, and resilience to extended grid outages, can be engineered using locally available materials and components.

Compliance with ethical standards

Disclosure of conflict of interest

No conflict of interest to be disclosed.

References

[1] N. J. Todd, “Hospital Beds,” *JAMA*, vol. 334, no. 12, p. 1118, Sep. 2025, doi: 10.1001/jama.2025.8319.

[2] J. B. Awotunde, “Introduction to smart hospital,” in *Blockchain and Digital Twin for Smart Hospitals*, Elsevier, 2025, pp. 1–35. doi: 10.1016/B978-0-443-34226-4.00002-2.

[3] M. R. F. https://www.marketresearchfuture.com, “Smart Hospital Market Size, Share Report and Trends 2035.” Accessed: Apr. 30, 2026. [Online]. Available: https://www.marketresearchfuture.com/reports/smart-hospital-market-4505

[4] H. E. Aloh, O. E. Onwujekwe, O. G. Aloh, and C. J. Nweke, “Is bed turnover rate a good metric for hospital scale efficiency? A measure of resource utilization rate for hospitals in Southeast Nigeria,” *Cost Eff. Resour. Alloc.*, vol. 18, no. 1, p. 21, Dec. 2020, doi: 10.1186/s12962-020-00216-w.

[5] M. Recmanik *et al.*, “A Review of Patient Bed Sensors for Monitoring of Vital Signs,” *Sensors*, vol. 24, no. 15, p. 4767, Jul. 2024, doi: 10.3390/s24154767.

[6] A. Theodosiou, “Recent Advances in Fiber Bragg Grating Sensing,” *Sensors*, vol. 24, no. 2, p. 532, Jan. 2024, doi: 10.3390/s24020532.

[7] M. Bruyneel, W. Libert, and V. Ninane, “Detection of bed-exit events using a new wireless bed monitoring assistance,” *Int. J. Med. Inf.*, vol. 80, no. 2, pp. 127–132, Feb. 2011, doi: 10.1016/j.ijmedinf.2010.10.007.

[8] S. Zeadally and O. Bello, “Harnessing the power of Internet of Things based connectivity to improve healthcare,” *Internet Things*, vol. 14, p. 100074, Jun. 2021, doi: 10.1016/j.iot.2019.100074.

[9] “ISO/IEEE 11073-10206:2024(en), Health informatics — Device interoperability — Part 10206: Personal health device communication — Abstract content information model.” Accessed: Apr. 30, 2026. [Online]. Available: https://www.iso.org/obp/ui/es/#iso:std:iso-ieee:11073:-10206:ed-1:v1:en

[10] J. H. Kim, N. Theodore, R. Iyer, A. Manbachi, and R. Um, “Development of Voice-Controlled Smart Surgical Bed,” in *2020 Design of Medical Devices Conference*, Minneapolis, Minnesota, USA: American Society of Mechanical Engineers, Apr. 2020, p. V001T10A012. doi: 10.1115/DMD2020-9065.

[11] A. R. Zubair, “Biomedical instruments: safety, quality control, maintenance, prospects and benefits of African technology,” *African journal of medicine and medical sciences*, vol. 39, pp. 35–40, 2010.

[12] S. Abdulmalek *et al.*, “IoT-Based Healthcare-Monitoring System towards Improving Quality of Life: A Review,” *Healthcare*, vol. 10, no. 10, p. 1993, Oct. 2022, doi: 10.3390/healthcare10101993.

[13] A. R. Zubair and A. O. Ogunware Telediagnosis: Interfacing Biomedical Diagnostic Devices with Internet of Things (IoT) using ThingsSpeak Web-Based Platform. *In:* D. P. Asante, R. Boatang, L. O. Babatope and A, Okunoye (Eds.). *Proceedings of the 13th ISTEAMS Cross-Border Conference* 24-26 October, 2018. Accra. 141–150pp.

[14] K. Soyemi and A. T.Aborode, A. T. (2022). Hospital bed shortage and overcrowding in Nigerian tertiary healthcare centers: Challenges and implications for emergency care. *African Journal of Emergency Medicine, 12*(2), 156–163, 2022.

[15] R. L. Ibrahim, K. Bello. Ajide, and O. Olatunde Julius, “Easing of lockdown measures in Nigeria: Implications for the healthcare system,” *Health Policy Technol.*, vol. 9, no. 4, pp. 399–404, Dec. 2020, doi: 10.1016/j.hlpt.2020.09.004.

[16] A. R. Zubair, I. I. Ojiodu and B. O. Abideen COVID-19 Management Requires Self-Sufficiency of Nations During Lockdown: Local Development of Body Mass Index Machine. *Journal of Multidisciplinary Engineering Science Studies,* Vol. 7. No. 10: 4062-4075, 2021.

[17] O. Adeodu, “Anthropometry as ergonomic consideration for hospital bed design in Nigeria,” 2014. Accessed: Apr. 30, 2026. [Online]. Available: https://www.semanticscholar.org/paper/Anthropometry-as-ergonomic-consideration-for-bed

[18] “Ergonomic Evaluation of Hospital Bed Design and Anthropometric Characterization of Adult Patients in Nigeria,” 2016. Accessed: Apr. 30, 2026. [Online]. Available: https://www.semanticscholar.org/paper/Ergonomic-Evaluation-of-Hospital-Bed-Design-